Robust Speed Regulation for PMSM Servo System With Multiple Sources of Disturbances via an Augmented Disturbance Observer

Yunda Yan, *Student Member, IEEE*, Jun Yang, *Member, IEEE*, Zhenxing Sun, *Member, IEEE*, Chuanlin Zhang, *Member, IEEE*, Shihua Li, *Senior Member, IEEE*, and Haoyong Yu, *Member, IEEE*

***Abstract*—Permanent magnet synchronous motors are extensively used in high-performance industrial applications. However, plenty of practical factors (e.g., cogging torques, load torques, friction torques, measurement error effects, dead-time effects, and parameter perturbations) in the closed-loop servo system inevitably bring barriers to the high-performance speed regulation, which can be regarded as generalized disturbances. Most of the existing control approaches only focus on one single kind of disturbances. However, the practical servo system is affected by multiple sources of disturbances simultaneously and these disturbances enter into the system through different channels. To this end, this paper systematically analyzes several representative disturbances, particularly including their features and distribution in the practical servo system, and then, specifically puts forward a novel disturbance rejection framework based on a noncascade structure. Under this framework, a comprehensive disturbance observer is proposed to simultaneously and accurately estimate multiple disturbances such that a composite controller can be designed to correspondingly compensate disturbances. Rigorous analysis of stability is established. Comparative experimental results demonstrate that the proposed method achieves a better speed dynamic response and a higher accuracy tracking performance even in the presence of multiple sources of disturbances.**

***Index Terms*—Disturbance modeling, disturbance observer, multiple disturbances, permanent magnet synchronous motor (PMSM), robust control.**

Manuscript received November 27, 2016; revised February 17, 2017, April 29, 2017, July 11, 2017, and September 29, 2017; accepted January 21, 2018. Date of publication January 30, 2018; date of current version April 16, 2018. Recommended by Technical Editor S. K. Dwivedi. This work was supported in part by the National Natural Science Foundation of China under Grant 61473080, Grant 61503236, Grant 61573099, Grant 61633003, and Grant 61750110525, in part by the Fundamental Research Fund for the Central Universities under Grant 2242016R30011, in part by the State Scholarship Fund under Grant 201706090111, in part by the Biomedical Research Council (BMRC) under Grant 15/12124019 from the Agency for Science, Technology, and Research (A*STAR), Singapore, and in part by the National Medical Research Council under Grant NMRC/BnB/0019b/2015, Ministry of Health, Singapore. *(Corresponding author: Shihua Li.)*

Y. Yan, J. Yang, and S. Li are with the Key Laboratory of Measurement and Control of Complex Systems of Engineering (CSE), Ministry of Education, School of Automation, Southeast University, Nanjing 210096, China (e-mail: yyd@seu.edu.cn; j.yang84@seu.edu.cn; lsh@seu.edu.cn).

Z. Sun is with the College of Electrical Engineering and Control Science, Nanjing Tech University, Nanjing 211816, China (e-mail: snzhenxing@hotmail.com).

C. Zhang is with the College of Automation Engineering, Shanghai University of Electric Power, Shanghai 200090, China (e-mail: clzhang@shiep.edu.cn).

H. Yu is with the Department of Biomedical Engineering, Faculty of Engineering, National University of Singapore, Singapore 117576 (e-mail: bieyhy@nus.edu.sg).

Color versions of one or more of the figures in this paper are available online at http://ieeexplore.ieee.org.

Digital Object Identifier 10.1109/TMECH.2018.2799326

I. Introduction

In VIRTUES of high efficiency, high power density, and large torque-to-inertia ratio [1], permanent magnet synchronous motors (PMSMs) have been receiving abundant attention and extensively applied to plenty of practical industrial applications, e.g., robotics, power generations, and aerospace [2]–[5]. In these applications, superior dynamic response and high-accuracy tracking performance are of great significance.

However, it is worth noting that its performance qualities are always diminished by various disturbances/uncertainties. In a typical PMSM servo system, the basic components include a controller, Hall current sensors, an encoder, an inverter module, and a motor. Each one unavoidably generates disturbances/uncertainties. How to attenuate these adverse effects is therefore one of the most crucial issues that should be considered by practitioners. In recent years, lots of advanced control approaches have been put forward to promote its disturbance rejection ability.

1) *Current Sensor:* To handle the offset error in phase current measurements, a cascade model predictive control scheme with an embedded disturbance model is proposed in [3] and a robust two degrees of freedom speed regulator based on the internal model principle is developed in [5].
2) *Encoder:* In [6], a generalized proportional integral observer based control (GPIOBC) method is used to suppress the effect of the offset error in angular measurement.
3) *Inverter Module:* In [7], a control scheme using two linear extended state observers is proposed to inhibit the dead-time effect in space vector pulse-width modulation (SVPWM) signals.
4) *Motor:* Speed/torque ripples caused by flux harmonics, current measurement errors, and cogging torques are min-

imized by iterative learning control method in [8]. In [9], a Luenberger version of observer is used to estimate and then compensate the periodic torque disturbances in the motor. The effect of inertia variation is suppressed by an adaptive control scheme based on parameter identification in [10]. In [11], an adaptive disturbance observer is designed to estimate the lumped uncertainty caused by parameter variations and flux harmonics, and corresponding feedforward compensation based upon the estimates is utilized to approximately cancel it.

5) *External Torque:* Unknown constant or slowly varying load torques are rejected by linear disturbance observer based control methods in [4], [10], [12]–[14]. In [15], a continuous nonsingular terminal sliding mode controller combined with finite-time disturbance observer is proposed to handle unknown time-varying load torques. In [16], an adaptive fuzzy controller is introduced to cope with nonlinear friction torque.

However, due to the complex features and intricate distribution, all these disturbances/uncertainties in the whole system are not easy to be attenuated by the above-mentioned control methods. To the best of authors' knowledge, most of the published papers focus on attenuating part(s) of disturbances/uncertainties generated in certain single component of the servo system, rather than considering them as a whole within the closed-loop plant.

To address the above-mentioned challenges, we propose a robust speed control law to improve the multiple disturbance rejection ability of the whole PMSM servo system. Compared with the previous related results, the main contributions of this paper are summarized by the following two aspects.

1) *Refined Disturbance Modeling:* Representative disturbances/uncertainties associated within motor body, Hall sensors, and actuators are all considered and explicitly modeled in this paper. These uncertain factors come from a wide range of sources and are definitely exhibited as various features, which finally bring huge barriers to high-performance control of the servo system.
2) *Multiple Disturbance Attenuation:* By virtue of the output regulation theory [17], [18], the involved dynamic PMSM system is transformed to a relatively simple one with only the matched disturbances. By making use of internal models of disturbances, a comprehensive disturbance observer is designed to estimate the multiple disturbances. With the disturbance estimates, a universal robust speed regulation framework is presented.

Besides, comparative experimental studies with proportional-integral-derivative (PID) method, GPIOBC method [6], and basic harmonic disturbance observer based control (HDOBC) method [19] are carried out to demonstrate both effectiveness and feature of the proposed method.

II. Preliminaries

A. Dynamic Model of Ideal PMSM

A generic ideal model of PMSM in the rotating reference frame is given as follows [20]:

$$\begin{aligned}\frac{di_d}{dt} &= \frac{1}{L_d}(u_d - R_s i_d + n_p \omega L_q i_q)\\ \frac{di_q}{dt} &= \frac{1}{L_q}(u_q - R_s i_q - n_p \omega L_d i_d - n_p \omega \psi_f)\\ \frac{d\omega}{dt} &= \frac{1}{J}(T_e - T_f - T_L)\\ \frac{d\theta_e}{dt} &= n_p \omega \end{aligned} \tag{1}$$

where θ_e is the electrical angle; ω is the rotor angular velocity; i_d and i_q are d- and q-axis stator currents, respectively; u_d and u_q are d- and q-axis stator voltages, respectively; L_d and L_q are d- and q-axis stator inductances, respectively; ψ_f is the magnetic flux linkage; R_s is the stator resistance; J is the moment of the total inertial (motor and load); B_v is the viscous frictional coefficient; n_p is the number of pole pairs; T_e is the electromagnetic torque $3/2 n_p[\psi_f i_q + (L_d - L_q) i_d i_q]$; T_f is the friction torque $B_v \omega$; and T_L is the load torque.

B. Analysis of Disturbances/Uncertainties in Practical PMSM Servo Systems

Unlike the ideal model (1), a practical PMSM servo system face multiple sources of disturbances/uncertainties, which will be classified and briefly reviewed as follows.

1) Unmodeled Dynamics: The unmodeled dynamics in a PMSM servo system is mainly the result of the unique motor body structure (e.g., cogging torque [21], [22], high-order back-electromotive force (EMF) harmonics [8], [23], and slot harmonics [24]), the loss of control output producing (e.g., dead-time effects [7], [25] and inverter voltage drops [26]), the errors of information acquisition (e.g., measurement error effects [3], [5], [6], [8], [27]), and the unstructured uncertainties due to mechanical factors (e.g., misalignment of shaft, broken shaft, and twisted shaft [28]).

2) Parametric Uncertainties: Parameters of PMSM can be divided into mechanical (J, B_v, and ψ_f) and electrical ones (R_s, L_d, and L_q). Both of them are time varying in most cases. For example, inertia J (including both motor and load) increases as time goes by in electric winding machine [2], stator resistance R_s varies primarily with temperature [23] and stator inductances L_d and L_q vary with time due to the effects of cross saturation [29].

3) External Disturbances: Load torque is generally regarded as the most serious disturbance for high performance [4], [10], [12]–[14]. Speed will inevitably fluctuate when load torque is imposed on or evacuated from the motor. Besides, undesirable effects caused by friction torque also widely exist in a PMSM servo system [16], [20], [30]–[34].

It is worth noting that all the disturbances/uncertainties appear in the closed-loop servo system, from the motor itself to sensors and actuators, as shown in Fig. 1. The motivation of this paper is to design a control law to uniformly suppress most of these disturbances/uncertainties. To this end, we first try our best to model, estimate, and compensate disturbances/uncertainties and then the rest unmodeled ones are suppressed in a robust approach.

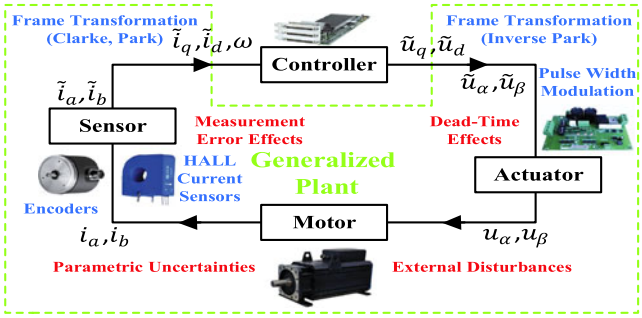

Fig. 1. Disturbance distribution in the closed-loop servo system.

Remark 1: In most of the published results [2], [4], [10]–[15], only the ideal model (1) is considered, ignoring many practical characteristics of sensors, actuators, and motor bodies. Based on such an ideal model, how to suppress load torques or parametric uncertainties is the major concern. However, without considering these nonideal characteristics, it is not easy to achieve the desired performances of PMSM. As a consequence, it is necessary to understand the concept of "generalized plant" as accurate as possible before designing the controller. As shown in Fig. 1, the basic components of a typical PMSM servo system include a controller, Hall current sensors, an encoder, an inverter module, and a motor. The "generalized plant" is in other parts of the closed-loop servo system except the controller. In other words, the full closed-loop dynamic model rather than the ideal one is considered in this paper, which is more practical and meaningful.

Remark 2: Due to technical constraints, it is not easy to imitate all kinds of disturbances/uncertainties by the current experimental setup. Therefore, as representatives in this paper, current measurement error effects in sensor, dead-time effects in actuator, and cogging/load torques in motor are specifically analyzed and exactly compensated while the rest (e.g., parametric perturbation, high-order back-EMF harmonics, and nonlinear part of friction torques) are considered as unmodeled dynamics and are suppressed in a robust way. More information about these unmodeled dynamics is introduced in [2], [8], [16], [20], [23], [24], [26], [29], [28], and [31]–[34]. In several higher performance servo application areas, it is recommended that the proposed control method can be extended to improve the robustness performance against the rest unmodeled dynamics by systematically modeling these disturbances/uncertainties.

C. Generalized Plant Modeling

To model the "generalized plant," the following transformation (2) is first utilized:

$$\tilde{i}_q = i_q + i_q^{\text{offset}} + i_q^{\text{scaling}}, u_q = \tilde{u}_q + u_q^{\text{dead}}, \tilde{T}_e = T_e + T^{\text{cog}} \tag{2}$$

where $\tilde{i}_q$ is q-axis current obtained from the measured phase currents, $\tilde{u}_q$ is the output voltage of the controller, and $\tilde{T}_e$ is the practical electromagnetic torque.

1) Current Measurement Error Effect: i_q^{offset} and i_q^{scaling} are the equivalent disturbances on q-axis current due to the offset and the scaling errors in phase current measurements and have been modeled in detail in [27]: $i_q^{\text{offset}} = i^{\text{offset}} \cos(\theta_e + \alpha), i_q^{\text{scaling}} = i^{\text{scaling}} [\cos(2\theta_e + \beta) + 1/2]$ where i^{offset} and i^{scaling} are the amplitudes of ripples and α and β are the constant angular displacements.

2) Dead-Time Effect: u_q^{dead} is the distortion of q-axis voltage due to the dead-time effects and has been modeled in detail in [25]: $u_q^{\text{dead}} = \sum_{i=0}^{\infty} u^{\text{qi}} \cos 6i\theta_e$ where u^{qi} is its $6i$ th-order harmonic amplitude.

3) Cogging Torque: T^{cog} is the cogging torque and has been modeled in detail in [22]: $T^{\text{cog}} = \sum_{i=1}^{\infty} T^{\text{cogi}} \cos(iQ\theta_m + \varphi_i)$ where $\theta_m = \theta_e / n_p$ is the mechanical angular position of the rotor, Q is the number of the slots, and T^{cogi} and φ_i are the corresponding amplitude and phase angle.

Thus, parts of system (1) can be rewritten as the following system:

$$\begin{aligned} \frac{d}{dt}\tilde{i}_q &= -\frac{R_s}{L_q}\tilde{i}_q - \frac{n_p\psi_f}{L_q}\omega - \frac{n_p\omega L_d \tilde{i}_d}{L_q} + \frac{1}{L_q}\tilde{u}_q + d_q + \varepsilon_q \\ \frac{d}{dt}\omega &= \frac{3n_p\psi_f}{2J}\tilde{i}_q - \frac{B_v}{J}\omega + d_\omega + \varepsilon_\omega \end{aligned} \tag{3}$$

where $\tilde{i}_d$ is d-axis current obtained from the measured phase currents; d_q and d_ω represent the main external and internal disturbances in q-axis current loop and speed loop, expressed as $d_q \triangleq (d/dt + R_s/L_q) i_q^{\text{offset}} + (d/dt + R_s/L_q) i_q^{\text{scaling}} + \tilde{u}_q^{\text{dead}}/L_q, d_\omega \triangleq -3n_p\psi_f/(2J) i_q^{\text{offset}} - 3n_p\psi_f/(2J) i_q^{\text{scaling}} + \tilde{T}^{\text{cog}}/J - \tilde{T}_L/J, \tilde{u}_q^{\text{dead}} \triangleq u^{\text{q0}} + u^{\text{q1}} \cos 6\theta_e$, $\tilde{T}^{\text{cog}} \triangleq T^{\text{cog1}} \cos(Q\theta_m + \varphi_1), \tilde{T}_L \triangleq \sum_{i=0}^{N_{T_L}} c_i t^i$, $c_i \triangleq 1/i! \cdot d^i T_L/dt^i|_{t=0}$; ε_q and ε_ω are the lumped uncertainties in q-axis current loop and speed loop, expressed as $\varepsilon_q \triangleq (u_q^{\text{dead}} - \tilde{u}_q^{\text{dead}})/L_q + f_q, \varepsilon_\omega \triangleq (T^{\text{cog}} - \tilde{T}^{\text{cog}})/J - (T_L - \tilde{T}_L)/J + 3n_p(L_d - L_q)/(2J) i_d i_q + f_\omega$; and f_q and f_ω are the lumped effects of parametric perturbation and other unmodeled disturbances/uncertainties.

System (3) represents the generalized model of PMSM servo system under multiple sources of disturbances via the available information by sensors. It becomes clear that system (3) is affected by various disturbances/uncertainties through different channels, i.e, q-axis current and speed channels. Worse still, these disturbances are expressed in different forms, i.e., polynomial and periodical. All these factors impose a great challenge for attenuating multiple disturbances.

Remark 3: In the steady state, i.e., the motor is approximatively running at a constant speed ($\omega \approx \omega^*$), electrical angle θ_e approximately equals $n_p\omega^* t + \alpha_\omega$ where α_ω is a constant angular displacement, leading to the fact that the frequencies of oscillations in d_q and d_ω are approximately fixed. This reasonable inference simplifies the problem, as frequencies of periodical signals in d_q and d_ω can be available according to mechanism or signal analysis. For example, the frequency of oscillation in the steady state caused by the offset phase current measurement errors is $n_p\omega^*/(2\pi)$(Hz) and $n_p\omega^*/\pi$(Hz) is that of the scaling phase current measurement errors.

III. Control Strategy

A. Composite Controller Design

Before the controller design, the following transformation (4) is obtained to simplify the model:

$$x_1 = \pi_\omega - \omega, x_2 = \pi_{\tilde{i}_q} - \tilde{i}_q \tag{4}$$

where $\pi_\omega \triangleq \omega^*$ and $\pi_{\tilde{i}_q} \triangleq 2B_v\omega/(3n_p\psi_f) - 2Jd_\omega/(3n_p\psi_f) - 2J\varepsilon_\omega/(3n_p\psi_f)$. System (3) is then transformed as follows:

$$\dot{x}_1 = \frac{3n_p\psi_f}{2J}x_2, \dot{x}_2 = \left(-\frac{B_v}{J} - \frac{R_s}{L_q}\right)x_2 - \frac{1}{L_q}(\tilde{u}_q - \pi_{\tilde{u}_q}) \tag{5}$$

where

$$\pi_{\tilde{u}_q}/L_q \triangleq \underbrace{[2B_vR_s/(3n_p\psi_fL_q) + n_p\psi_f/L_q + n_pL_d\tilde{i}_d/L_q]\omega}_{\text{Direct Compensation}}$$
$$\underbrace{-u^{q1}\cos 6\theta_e + [-2/(3n_p\psi_f)d/dt - 2R_s/(3n_p\psi_fL_q)] \cdot T^{cog1}\cos(Q\theta_m + \varphi_1)}_{\text{Harmonic Components}}$$
$$\underbrace{-u^{q0} + [2/(3n_p\psi_f)d/dt + 2R_s/(3n_p\psi_fL_q)]\sum_{i=0}^{N_{T_L}} c_it^i}_{\text{Polynomial Components}}$$
$$\underbrace{-\varepsilon_q + [-2J/(3n_p\psi_f)d/dt - 2JR_s/(3n_p\psi_fL_q)]\varepsilon_\omega}_{\text{Unmodeled Dynamics}}.$$

To compensate $\pi_{\tilde{u}_q}$, $\tilde{u}_q$ is divided into two parts, direct one $\tilde{u}_{qd}$ and indirect one $\tilde{u}_{qi}$ where

$$\tilde{u}_{qd} = \left(\frac{2B_vR_s}{3n_p\psi_f} + n_p\psi_f + n_pL_d\tilde{i}_d\right)\omega \tag{6}$$

is the direct compensation control for viscous friction, back-EMF, and coupling based on PMSM's normal parameters, whereas $\tilde{u}_{qi}$ is the indirect compensation control for other unknown disturbances/uncertainties, which will be designed later.

Remark 4: In transformation (4), we try to force the steady-state responses to the desired ones, which is the basic idea in the output regulation method [17], [18]. Here, the desired steady states are calculated by assuming that the speed tracks the given reference offset free and all the disturbances/uncertainties are available. It is obvious that π_ω and $\pi_{\tilde{i}_q}$ are the desired steady states, whereas x_1 and x_2 are the errors between the states and the desired ones. By this transformation, multiple sources of matched and mismatched disturbances in original system (3) are equivalent to the matched one in system (5). Therefore, the desired steady state $\pi_{\tilde{u}_q}$ is also referred to as the equivalent input disturbance [35].

Based on the above-mentioned mechanism analysis, the considered internal disturbance models are immersed into system (5). We first define $x_3 \triangleq -u^{q1}\cos 6\theta_e$, $x_5 \triangleq [-2/(3n_p\psi_f)d/dt - 2R_s/(3n_p\psi_fL_q)]T^{cog1}\cos(Q\theta_m + \varphi_1)$, and $x_7 \triangleq (\pi_{\tilde{u}_q} - \tilde{u}_{qd})/L_q - x_3 - x_5$. Besides, since the frequencies of disturbances are approximatively available according to the reference speed by Remark 3, the extended system is then represented as follows:

$$\begin{aligned}
\dot{x}_1 &= \frac{3n_p\psi_f}{2J}x_2 \\
\dot{x}_2 &= \left(-\frac{B_v}{J} - \frac{R_s}{L_q}\right)x_2 + x_3 + x_5 + x_7 - \frac{1}{L_q}\tilde{u}_{qi} \\
\dot{x}_3 &= x_4, \quad \dot{x}_4 = -(6n_p\omega^*)^2x_3 \\
\dot{x}_5 &= x_6, \quad \dot{x}_6 = -(Q\omega^*)^2x_5 \\
\dot{x}_7 &= x_8, \quad \ldots, \quad \dot{x}_{i+6} = x_7^{(i)}
\end{aligned} \tag{7}$$

where x_3 is the lumped dead-time effect, x_5 is the lumped effect of the cogging torque, and x_7 is the lumped effect of the load torque and other uncertainties.

Remark 5: Due to its limited bandwidth, the actual system is less affected by higher order harmonic disturbances. Therefore, these components are only regarded as part of the lumped disturbance x_7 in system (7), ignoring their internal models.

Taking into account the fact that multiple sources of disturbances exist in PMSM, disturbance observer is the first choice to accurately estimate them. This technology, initiatively put forward by Prof. K. Ohnishi and his colleagues in 1983 [36], has been successfully applied in various industrial sectors, especially motion control systems [31], [33], [37]–[42]. To estimate disturbances, Assumption 1 has to be satisfied.

Assumption 1: There exist positive constants $\gamma_{qi}, \gamma_{\omega j}, N_q \in \mathbb{N}$, and $N_\omega \in \mathbb{N}$ such that $|\varepsilon_q^{(i)}| \le \gamma_{qi}$ and $|\varepsilon_\omega^{(j)}| \le \gamma_{\omega j}, \forall i, j \in \mathbb{N}, i \ge N_q, j \ge N_\omega$.

By continually taking the derivative of x_7, its polynomial components are vanished. Finally, one gets that $x_7^{(N)} = -\varepsilon_q^{(N)} - 2J/(3n_p\psi_f)\varepsilon_\omega^{(N+1)} - 2JR_s/(3n_p\psi_fL_q)\varepsilon_\omega^{(N)}$ where $N \triangleq \max\{N_q, N_\omega, N_{T_L}, 1\}$. If Assumption 1 is satisfied, we then have $|x_7^{(N)}| \le \gamma_{qN} + 2J/(3n_p\psi_f)\gamma_{\omega(N+1)} + 2JR_s/(3n_p\psi_fL_q)\gamma_{\omega N}$. Similarly, the following corollary is obvious.

Corollary 1: Under Assumption 1, there exist positive constants γ_i such that $|x_7^{(i)}| \le \gamma_i, \forall i \in \mathbb{N}, i \ge N$.

In this paper, a reduced-order disturbance observer integrating internal models of disturbances is designed as follows:

$$\begin{aligned}
\dot{z}_2 &= \left[l_2\left(\frac{B_v}{J} + \frac{R_s}{L_q}\right) - l_2^2 - l_3 - l_5 - l_7\right]\frac{2J}{3n_p\psi_f}x_1 \\
&\quad + \left(l_2 - \frac{B_v}{J} - \frac{R_s}{L_q}\right)z_2 + z_3 + z_5 + z_7 - \frac{1}{L_q}\tilde{u}_{qi} \\
\dot{z}_3 &= (-l_2l_3 - l_4)\frac{2J}{3n_p\psi_f}x_1 + l_3z_2 + z_4 \\
\dot{z}_4 &= \left[-l_2l_4 + l_3(6n_p\omega^*)^2\right]\frac{2J}{3n_p\psi_f}x_1 + l_4z_2 - (6n_p\omega^*)^2z_3 \\
\dot{z}_5 &= (-l_2l_5 - l_6)\frac{2J}{3n_p\psi_f}x_1 + l_5z_2 + z_6 \\
\dot{z}_6 &= \left[-l_2l_6 + l_5(Q\omega^*)^2\right]\frac{2J}{3n_p\psi_f}x_1 + l_6z_2 - (Q\omega^*)^2z_5
\end{aligned}$$

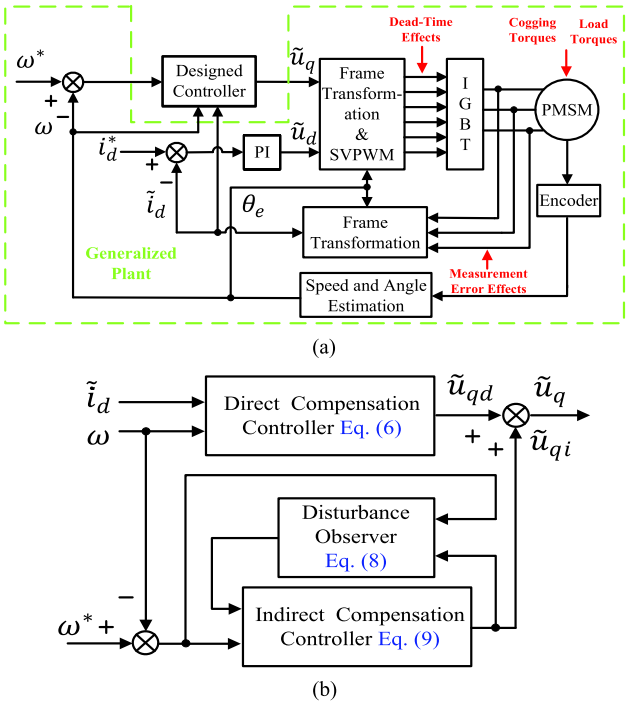

Fig. 2. Schematic diagram of the proposed method. (a) General drawing. (b) Designed controller.

$$\begin{aligned}
\dot{z}_7 &= (-l_2 l_7 - l_8)\frac{2J}{3n_p\psi_f}x_1 + l_7 z_2 + z_8 \\
&\cdots \\
\dot{z}_{N+6} &= -l_2 l_{N+6}\frac{2J}{3n_p\psi_f}x_1 + l_{N+6} z_2 \\
\hat{x}_i &= z_i - \frac{2J}{3n_p\psi_f}l_i x_1 \quad (i = 2, 3, \ldots, N+6)
\end{aligned} \tag{8}$$

where $\hat{x}_i$ are the estimates of x_i, z_i are the intermediate variables, and l_i are the observer gains.

By means of the above-mentioned estimates, a composite control law for $\tilde{u}_{qi}$ is designed as follows:

$$\tilde{u}_{qi} = k_1 x_1 + k_2 \hat{x}_2 + L_q(\hat{x}_3 + \hat{x}_5 + \hat{x}_7). \tag{9}$$

Finally, the actual control law is the sum of (6) and (9)

$$\tilde{u}_q = \tilde{u}_{qd} + \tilde{u}_{qi}. \tag{10}$$

In practice, constraints should be applied on the control inputs for protection, i.e., $|\tilde{u}_q|, |\tilde{u}_d| \le U_{\max}$. The schematic diagram of the proposed method is shown in Fig. 2.

Remark 6: The tuning guideline used for both controller gains k_i and observer gains l_i is based upon the scaling and bandwidth-parameterization method introduced in [43]. Due to the controllability and observability, both gains are analytically related to the eigenvalues of $\boldsymbol{\Phi}_{\boldsymbol{x}}$ and $\boldsymbol{\Phi}_{\boldsymbol{e}}$ in system (11) and this relationship can be explicitly obtained by "place" instruction in MATLAB. In [43], eigenvalues are suggested to be placed at multiple ones for tuning simplicity and the guideline of choosing these multiple eigenvalues is also introduced.

Remark 7: In the controller design, the coupling between d-axis current and speed is directly compensated in $\tilde{u}_{qd}$ while the coupling between d-axis current and q-axis current is estimated and then indirectly compensated by $\tilde{u}_{qi}$. Therefore, the effect of d-axis current on speed is weakened to a large extent. To save space, a proportional-integral controller is used for d-axis current.

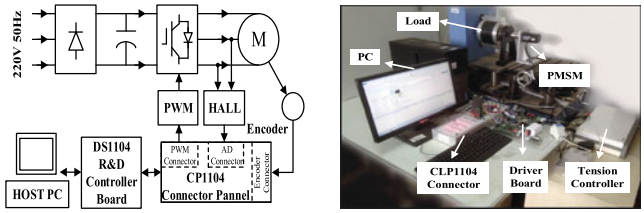

Fig. 3. Experimental system. (a) Configuration. (b) Setup.

B. Performance Analysis

Define $e_i \triangleq x_{i-1} - \hat{x}_{i-1}$ $(i = 3, 4, \ldots, N+7)$ as the estimation errors. Combining (9) into (7), the closed-loop system can be rewritten in a compact form as follows:

$$\dot{\boldsymbol{X}} = \boldsymbol{\Phi}\boldsymbol{X} + \boldsymbol{\Xi}d, y = \boldsymbol{\Gamma}\boldsymbol{X} \tag{11}$$

where variables are defined as $\boldsymbol{X} \triangleq [\boldsymbol{x}^\top \quad \boldsymbol{e}^\top]^\top, y \triangleq x_1, d \triangleq x_7^{(N)}, \boldsymbol{x} \triangleq [x_1 \quad x_2]^\top, \boldsymbol{e} \triangleq [e_3 \quad \cdots \quad e_{N+7}]^\top$ and matrices are defined as follows:

$$\boldsymbol{\Gamma} \triangleq \begin{bmatrix} 1 & \boldsymbol{0}_{1\times(N+6)} \end{bmatrix}, \boldsymbol{\Xi} \triangleq \begin{bmatrix} \boldsymbol{0}_{1\times(N+6)} & 1 \end{bmatrix}^\top$$

$$\boldsymbol{\Phi} \triangleq \begin{bmatrix} \boldsymbol{\Phi}_{x2\times 2} & \boldsymbol{\Phi}_{xe\,2\times(N+5)} \\ \boldsymbol{0}_{(N+5)\times 2} & \boldsymbol{\Phi}_{e\,(N+5)\times(N+5)} \end{bmatrix}$$

$$\boldsymbol{\Phi}_{\boldsymbol{x}} \triangleq \begin{bmatrix} 0 & 3n_p\psi_f/(2J) \\ -k_1/L_q & -B_v/J - R_s/L_q - k_2/L_q \end{bmatrix}$$

$$\boldsymbol{\Phi}_{\boldsymbol{xe}} \triangleq \begin{bmatrix} 0 & 0 & 0 & 0 & 0 & 0 & \boldsymbol{0}_{1\times(N-1)} \\ k_2/L_q & 1 & 0 & 1 & 0 & 1 & \boldsymbol{0}_{1\times(N-1)} \end{bmatrix}$$

$$\boldsymbol{\Phi}_{\boldsymbol{e}} \triangleq$$

$$\begin{bmatrix}
l_2 - B_v/J - R_s/L_q & 1 & 0 & 1 & 0 & 1 & 0 & 0 & \cdots & 0 \\
l_3 & 0 & 1 & 0 & 0 & 0 & 0 & 0 & \cdots & 0 \\
l_4 & -(6n_p\omega^*)^2 & 0 & 0 & 0 & 0 & 0 & 0 & \cdots & 0 \\
l_5 & 0 & 0 & 0 & 1 & 0 & 0 & 0 & \cdots & 0 \\
l_6 & 0 & 0 & -(Q\omega^*)^2 & 0 & 0 & 0 & 0 & \cdots & 0 \\
l_7 & 0 & 0 & 0 & 0 & 0 & 1 & 0 & \cdots & 0 \\
l_8 & 0 & 0 & 0 & 0 & 0 & 0 & 1 & \cdots & 0 \\
\vdots & \vdots & \vdots & \vdots & \vdots & \vdots & \vdots & \vdots & \ddots & \vdots \\
l_{N+5} & 0 & 0 & 0 & 0 & 0 & 0 & 0 & \cdots & 1 \\
l_{N+6} & 0 & 0 & 0 & 0 & 0 & 0 & 0 & \cdots & 0
\end{bmatrix}.$$

Our main results are given in the following theorem.

Theorem 1: Suppose that Assumption 1 is satisfied and observer gains l_i in (8) and control gains k_i in (9) are selected based upon Remark 6. The following statements hold.

1) Both the speed tracking and the disturbance estimation errors will converge to a bounded neighborhood of the origin and the ultimate bound can be made arbitrarily small.

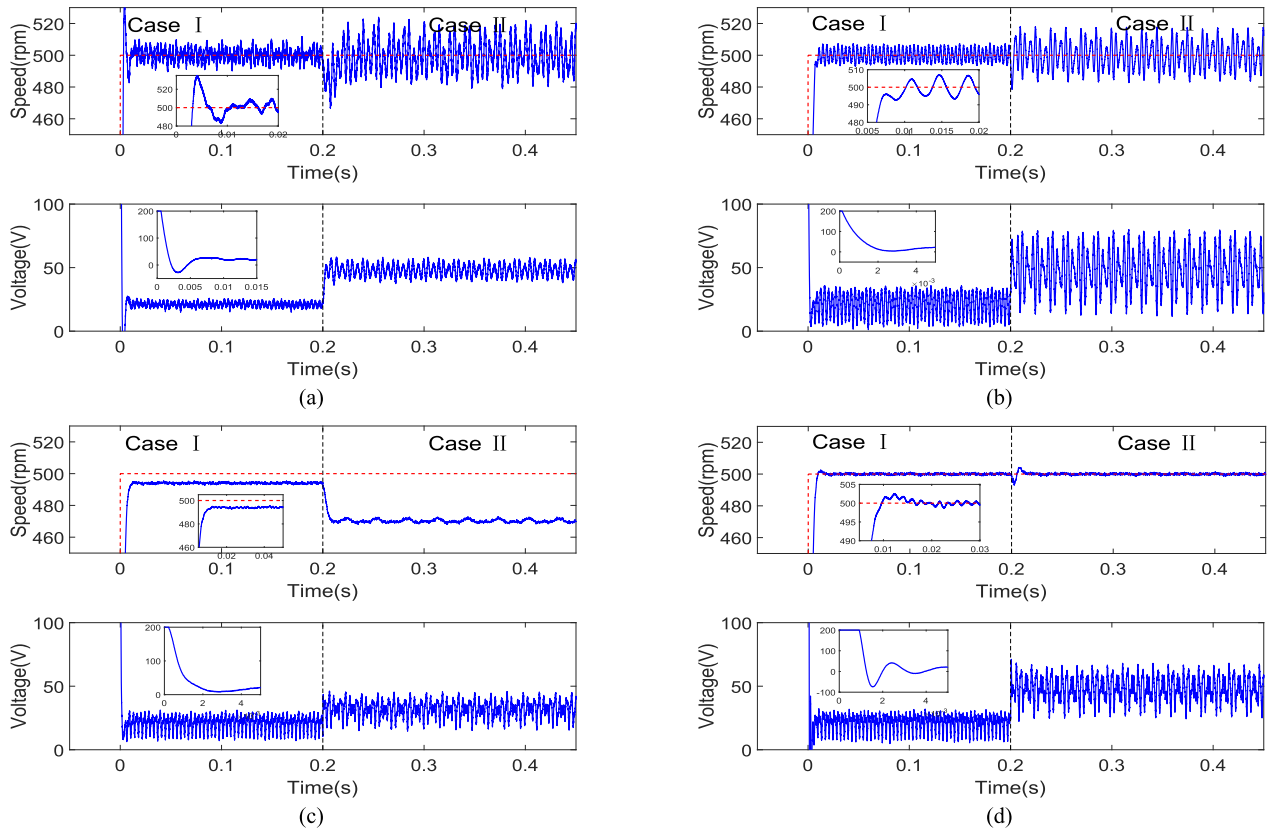

Fig. 4. Experimental performance comparisons of Cases I to II. (a) PID. (b) GPIOBC. (c) HDOBC. (d) CDOBC.

2) Moreover, if $x_7^{(N)}$ tends to zero as time goes to infinity, both the speed tracking and the disturbance estimation errors will then asymptotically converge to zero. A simple case is that both $\varepsilon_q^{(N)}$ and $\varepsilon_\omega^{(N)}$ tend to zero as time goes to infinity.

The proof of Theorem 1 is given in the appendix.

IV. Experimental Validation

To demonstrate the efficiency of the proposed method [named as comprehensive disturbance observer based control for convenience (CDOBC)], experiments on a PMSM servo system have been carried out. Both PID, GPIOBC [6], and HDOBC [19] algorithms are used to design q-axis controllers and tested on the PMSM servo system for comparisons.

The nominal parameters of the experimental PMSM are listed as follows: rated power $P_N = 200$ W, rated voltage $U_N = 220$ V, rated torque $T_N = 0.64$ N·m, rated current $I_N = 1.27$ A, rated speed $n_N = 3000$ r/min, number of pole pairs $n_p = 4$, number of slots $Q = 32$, rotor flux linkage $\psi_f = 0.084$ Wb, stator inductances $L_d, L_q = 26$ mH, stator resistance $R_s = 9.7\,\Omega$, rotor inertia $J = 1.35 \times 10^{-4}$ kg·m^2, and viscous friction coefficient $B_v = 7.4 \times 10^{-5}$ N·m·s/rad. The saturation limits of d-, q-axis voltages are both ± 200 V.

The experimental study is implemented by the setup in Fig. 3. Each control algorithm is implemented by dSPACE DS1104 control board, which is a completely real-time control system based on a 603 Power PC floating-point processor running at 250 MHz and offers a four-channel 16-b (multiplexed) analog to digital converter (ADC) and four 12-b ADC units. The power driving circuit is composed of single phase of diode bridge rectifier, large capacitor filter, and insulated gate bipolar transistor (IGBT) inverter. The current and voltage signals are detected by Hall sensors and an incremental encoder with 2500 lines is used to obtain the speed and position.

To fairly evaluate the control performance of the proposed method, parameters of controllers in all the four methods are chosen to make the system have a similar rising time via reaching the control limit (200 V). Control parameters in experiments are listed as follows: speed proportional, integral, and differential gains are 23, 10, and 0.0167 for PID method based on a noncascade structure; multiple eigenvalues of $\mathbf{\Phi}_{\boldsymbol{x}}$ and $\mathbf{\Phi}_{\boldsymbol{e}}$ are -200 and -520 for DOBC (GPIOBC, HDOBC, and CDOBC) methods; d-axis current proportional and integral gains are 120 and 240.

Remark 8: A noncascade structure is adopted here rather than the conventional double closed-loop structure. The constraint problem, especially the current constraint is crucial for the safety of the motor drives [20]. In general, specific mechanisms for handling state/control constraints should be taken into account. However, this paper mainly focuses on multiple disturbance modeling and attenuation in a practical PMSM servo system. Consequently, we do not pay too much attention on constraint handling, but claim that [44] provides a feasible way for the proposed method.

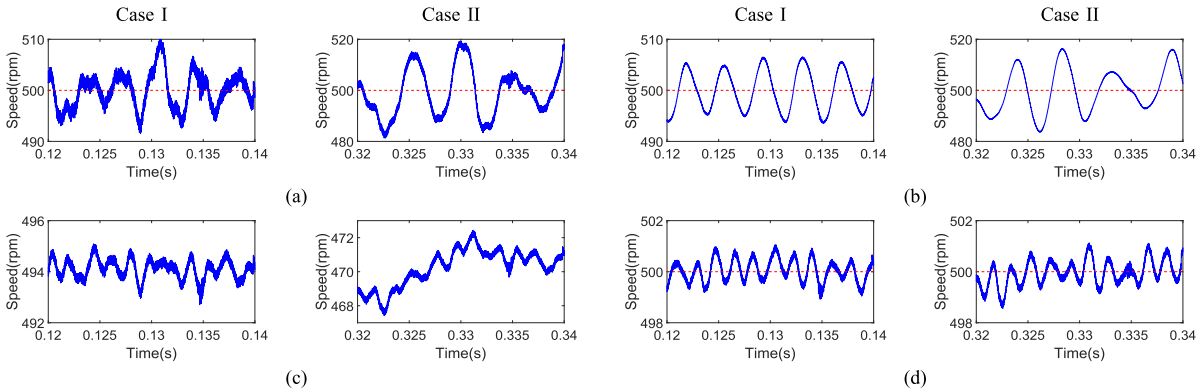

Fig. 5. Partial enlarged steady-state speed curves of Cases I to II. (a) PID. (b) GPIOBC. (c) HDOBC. (d) CDOBC.

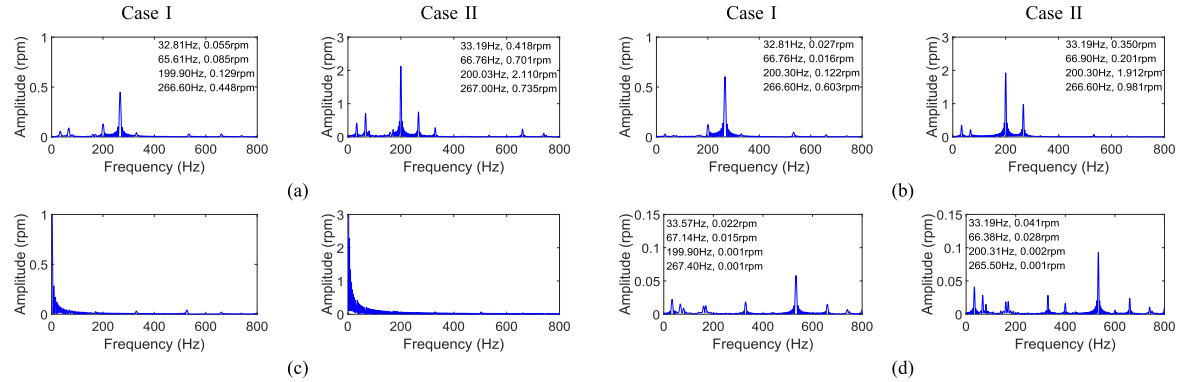

Fig. 6. Amplitude spectra of steady-state tracking error of Cases I to II. (a) PID. (b) GPIOBC. (c) HDOBC. (d) CDOBC.

A. Tracking Performance Without External Disturbances

In this subsection, dynamic state performances and tracking accuracies in the steady state of PMSM under all the four methods are thoroughly compared and studied. The robustness against various uncertainties (e.g., current measurement error effects, dead-time effects, and cogging torques) is the key factor determining the tracking accuracy. In order to obtain fair comparisons, experimental results of two cases are implemented as follows.

1) Case I considers a normal situation that is designed to verify the enhancement of the proposed method on the tracking accuracy.
2) Case II imitates the situation where relatively poor sensors and actuators are used.

In Case II, currents of -0.5 and 0.8 A and gains of 1.05 and 0.96 are respectively added on current measurements of phase A and phase B to magnify the offset and scaling current measurement effects while the dead time of inverters are changing from 3 μs in Case I to 7 μs to magnify the dead-time effects.

Case I—Tracking Performance in the Normal Situation: Fig. 4 shows the response curves of speed and q-axis voltage under all the four methods. The partial enlarged drawings of steady-state curves are correspondingly shown in Fig. 5. It can be observed that the system with CDOBC presents a shorter settling time, a smaller overshoot, and much smaller fluctuations in the steady state with almost no offset error. Even the system with HDOBC presents similarly small fluctuations, it cannot track reference speed offset free due to the unknown constant disturbance. To subtly analyze the factors of fluctuations, fast Fourier transformation is utilized. The amplitude spectra of the tracking errors are shown in Fig. 6. It can be concluded that the current measurement error effects (33.33, 66.67 Hz), the dead-time effects (200, 400, 800 Hz, ...), and the cogging torques (266.67, 533.33, 800 Hz, ...) of the system with CDOBC are suppressed to a large extent.

TABLE I
DYNAMIC-STATE AND STEADY-STATE PERFORMANCES

Index		PID	GPIOBC	HDOBC	CDOBC
Overshoot (%)		7	0.8	–	0.4
Settling time (ms)		22.4	18.7	21.9	17.6
Offset error (r/min)	Case I	0.0	0.0	−6.9	0.0
	Case II	0.0	0.0	−30.7	0.0
Fluctuation (r/min)	Case I	9.5	6.6	1.1	1.1
	Case II	21.0	17.2	1.9	1.3
Fluctuation rate (%)	Case I	1.9	1.3	0.2	0.2
	Case II	4.2	3.4	0.4	0.3

Case II—Tracking Performance in the Presence of Sensor/Actuator Errors: After 0.2 s, parts of internal disturbances are artificially magnified. It can be observed that the fluctuations of speed with both PID and GPIOBC and the offset error of speed with HDOBC are much larger than those in Case I. In Fig. 4(d), after a short transient process, the fluctuations of speed are almost recovered to the condition in Case I. This phenomenon

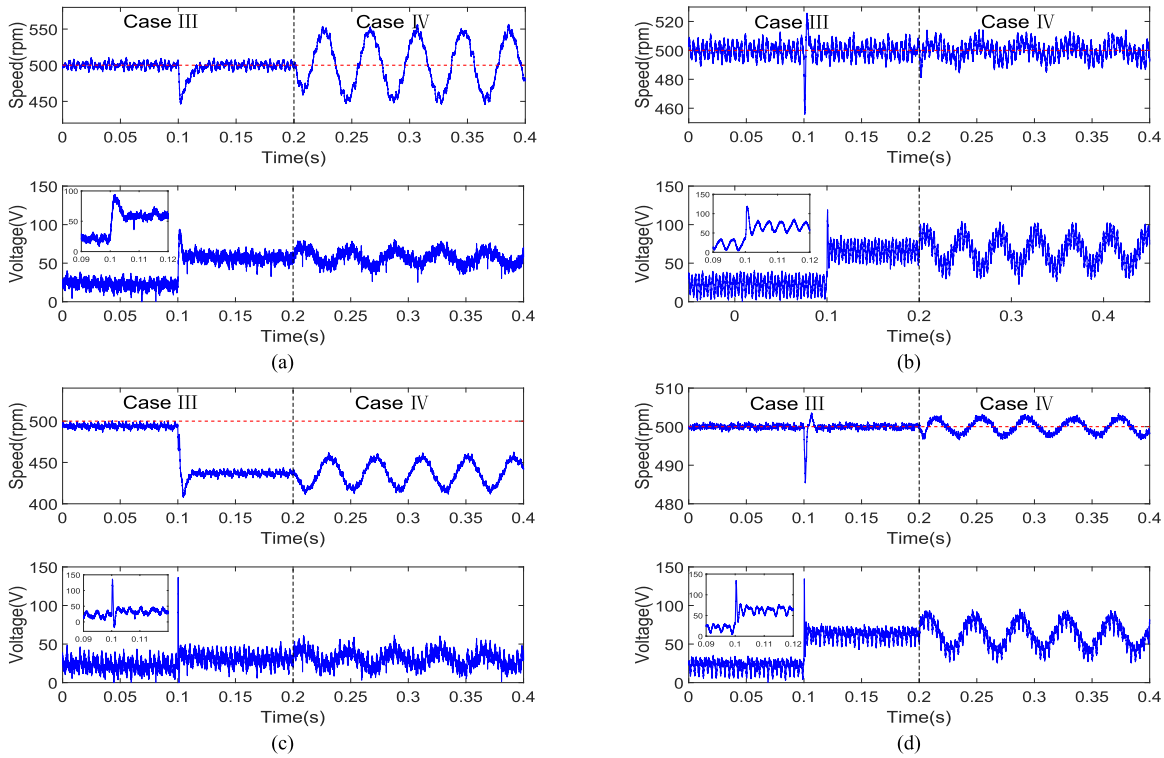

Fig. 7. Experimental performance comparisons of Cases III to IV. (a) PID. (b) GPIOBC. (c) HDOBC. (d) CDOBC.

implies that the proposed method largely improve the robustness of the servo system against current measurement error effects and dead-time effects. For further comparisons of the steady-state tracking performances, two indexes are introduced.

1) Fluctuation (r/min) $= (\omega_{\max} - \omega_{\min})/2$.
2) Fluctuation rate (%) $= (\omega_{\max} - \omega_{\min})/(\omega_{\max} + \omega_{\min}) \times 100$ where $\omega_{\max}$ and $\omega_{\min}$ are the maximum and the minimum of the steady-state speed, respectively.

Detailed quantitative data for performance comparisons of both cases are given in Table I. It can be observed from Table I that fluctuations on the speed curves of PID are relatively larger than those of HDOBC and CDOBC. The essential reason for this is referred to the internal model principle [45], i.e., the effects of disturbances can be completely attenuated if and only if the internal models of disturbances are incorporated into the controller design. This indicates that the PID controller can only remove the offset caused by constant/step disturbances since the integral action serves as the internal model of this kind disturbances.

B. Performance Evaluation Under Multiple Load Torques

In this section, the performances of disturbance rejection against time-varying load torques under all the four methods are compared, respectively. Two cases are also designed as follows.

1) Unknown constant/step load torques are imposed on the motor in Case III.

TABLE II
DISTURBANCE REJECTION PERFORMANCES AGAINST LOAD TORQUES

Index	PID	GPIOBC	HDOBC	CDOBC
Decrease (r/min)	53.7	44.3	87.6	14.6
Offset error (r/min)	0.3	−0.2	−62.6	0.0
Recovery time (ms)	38.6	19.1	23.2	14.5
Fluctuation (r/min)	53.8	12.7	23.4	3.2
Fluctuation rate (%)	10.7	2.5	5.4	0.6

2) Additional sine/cosine load torques with unknown frequencies, amplitudes, and phases are imposed in Case IV.

Case IV is designed to verify the robustness of the proposed method against periodic disturbances, which are not directly analyzed and handled by the presented mechanism. To obtain obvious results, the frequency of load torque in Case IV is chosen within the bandwidth of the system and the amplitude is chosen large enough. The load torques are given as follows:

$$T_L\,(\mathrm{N{\cdot}m}) = \begin{cases} 0 & 0 \le t < 0.1\,\mathrm{s} \\ 1.5 & 0.1\,\mathrm{s} \le t < 0.2\,\mathrm{s} \\ 1.5 + \sin(50\pi t) & 0.2\,\mathrm{s} \le t \le 0.4\,\mathrm{s}. \end{cases}$$

Case III—Recovery Performance Under Constant/Step Load Torque: Fig. 7 shows the speed and the q-axis voltage curves under all the four methods, respectively. It can be revealed that when a constant/step load torque 1.5 N·m is imposed on the motor at 0.1 s, the performance of CDOBC is much

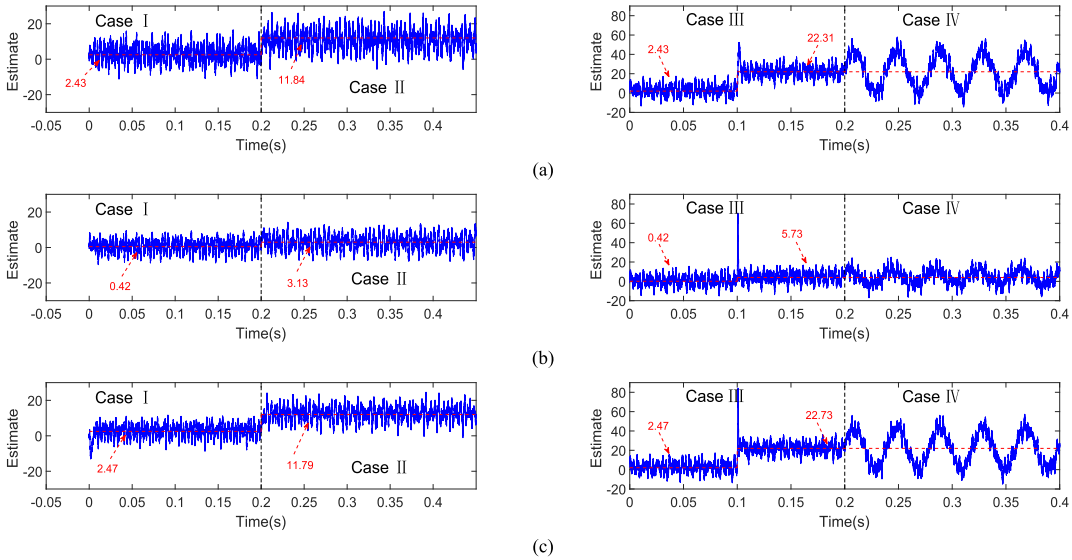

Fig. 8. Disturbance estimate of Cases I to IV. (a) GPIOBC. (b) HDOBC. (c) CDOBC.

better than others with the shortest settling time. Compared with CDOBC, the speed of HDOBC has similarly small fluctuations in Cases I to II; however, it cannot recover to its reference when load torque is imposed, as shown in Fig. 7(c). The reason is that this kind of method lacks internal model of the constant load disturbance. Besides, the speed of GPIOBC drops less and recovers faster than that of PID, but its fluctuations are relatively large in Cases I to II. The essential reason lies in the fact that the GPIOBC employs a robust disturbance observer to estimate the total disturbances roughly, which lacks of sufficient modeling analysis of the disturbances. As shown in Cases I to II, the system with CDOBC is more robust against internal disturbances than the other three methods.

Case IV—Recovery Performance Under Periodic Load Torque: Since that testing all kinds of disturbances is impossible, it is significant to design an experiment showing that the proposed method is robust enough against disturbances that are unmodeled and not directly conceived. To further compare the control performance, an additional sine/cosine load torque is imposed on the motor. In Fig. 7, it is obvious that the fluctuations of speed under CDOBC are much smaller than others. More detailed quantitative performance index comparisons of Cases III to IV are provided in Table II.

C. Effectiveness Validation of the Proposed Disturbance Observer

In this section, the effectiveness of different disturbance observers are discussed. First, it is worth noting that GPIO and HDO are two kinds of typical disturbance observers. GPIO is suitable for the case where almost no disturbance information is available; it is difficult to take full use of the available disturbance information. HDO works well when harmonic disturbances exist; however, if the practical disturbance dissatisfies this assumption, the performance will degrade. Compared with these two disturbance observers, the proposed approach is comprehensive and extensible. It fully utilizes the available disturbance information and exhibits strong robustness against unmodeled dynamics.

In Fig. 8, the experimental profiles of the disturbance estimates by different disturbance observers (GPIO, HDO, and CDO) are provided. In Case I, the disturbance estimates of GPIO and CDO are around 2.45, whereas that of HDO is 0.42, which leads to offset error in the steady state of HDOBC in Fig. 4. In Case III, when a constant/step load torque 1.5 N·m is imposed on the motor, the disturbance estimates of GPIO and CDO trend to around 22.52, whereas that of HDO is 5.73. This indicates why the speed of HDOBC cannot recover to its reference when constant/step load is imposed, as in Fig. 7.

Besides, it is obvious that the only difference of the three controllers (GPIOBC, HDOBC, and CDOBC) is the structure of their disturbance observers. Although the information of the disturbance estimation error is unavailable due to the unmeasured disturbances, the effectiveness of the proposed CDO still can be indirectly verified by the speed tracking comparisons in Cases I to IV.

V. Conclusion

The speed regulation problem for PMSM servo system with multiple sources of disturbances/uncertainties has been uniformly addressed in this paper. By combining the actual effects of both sensors and actuators into the dynamic model of PMSM, a generalized model has been built. A novel comprehensive disturbance observer embedded with internal disturbance/uncertainty models obtained by mechanism analysis has been applied to estimate the disturbances with higher accuracy. Controller with a corresponding compensation part for disturbances has been designed. Compared with PID and other DOBC methods, the proposed method has largely improved the performance for high-accuracy tracking and robustness against multiple sources of disturbances/uncertainties.

Future works will be concentrated on investigating and attenuating the adverse effects of nonlinear friction torque, sen-

sor noise, encoder quantization, and voltage/current saturation under the proposed control approach. Besides, the energy efficiency of the PMSM servo system is another interesting and promising research direction.

APPENDIX

This proof of Theorem 1 is divided into the following two parts.

1) The first is to prove that both the speed tracking and the disturbance estimation errors are bounded and tend to zero under a stronger assumption.
2) The second is to present the relationship between the ultimate bound of both the speed tracking and the disturbance estimation errors and the control parameters, which gives theoretical guidance for improving the tracking precision based on the proposed method.

A. Proof of the Bounded Speed Tracking and Disturbance Estimation Errors

Proof: Note that the eigenvalues of $\boldsymbol{\Phi}_{\boldsymbol{x}}$ and $\boldsymbol{\Phi}_{\boldsymbol{e}}$ can be placed in any locations of left half-plane. When $d(t) \equiv 0$, the closed-loop system (11) is then exponentially stable. Therefore, the closed-loop system (11) is input-to-state stable (ISS) with regard to $d(t)$.[1]

By the definition of ISS, there exist a class $\mathcal{KL}$ function β_1 and a class $\mathcal{K}$ function β_2 such that for any initial state $\boldsymbol{X}(t_0)$ and any bounded input $d(t)$, the solution $\boldsymbol{X}(t)$ exists for all $t \geq t_0$ and satisfies $\|\boldsymbol{X}(t)\| \leq \beta_1(\|\boldsymbol{X}(t_0)\|, t - t_0) + \beta_2(\sup_{t_0 \leq \tau \leq t}|d(\tau)|)$. This guarantees that for any bounded disturbance $d(t)$, both the tracking and the estimation errors will be bounded. Even as time goes to infinity, $\|\boldsymbol{X}(\infty)\| \leq \beta_2(\gamma_N) < \infty$.

Moreover, if $x_7^{(N)} = -\varepsilon_q^{(N)} - 2J/(3n_p\psi_f)\varepsilon_\omega^{(N+1)} - 2JR_s/(3n_p\psi_f L_q)\varepsilon_\omega^{(N)}$ tends to zero as time goes to infinity, i.e., $\lim_{t\to\infty} d(t) = 0$, the bound of both the tracking and the estimation errors will also goes to zero as time goes to infinity. ■

B. Proof of the Arbitrarily Small Speed Tracking and Disturbance Estimation Errors

First, we present the following definitions and lemma for concision.

Define $\boldsymbol{A} \triangleq \begin{bmatrix} \boldsymbol{0}_{(n-1)\times 1} & \boldsymbol{I}_{(n-1)\times(n-1)} \\ -1_{1\times 1} & \boldsymbol{\alpha}_{1\times(n-1)} \end{bmatrix} \in \mathbb{R}_{n\times n}$ where $\boldsymbol{\alpha} \triangleq -[\, C_n^{(n-1)} \; C_n^{(n-2)} \; \cdots \; C_n^1 \,] \in \mathbb{R}_{1\times(n-1)}$. Noting that $\boldsymbol{A}$ is Hurwitz matrix with -1 as its multiple eigenvalues, there exists a positive definite matrix $\boldsymbol{P} \in \mathbb{R}_{n\times n}$ such that $\boldsymbol{A}^\top\boldsymbol{P} + \boldsymbol{P}^\top\boldsymbol{A} = -\boldsymbol{I}$. Define $\lambda_{\max}(\boldsymbol{P})$ and $\lambda_{\min}(\boldsymbol{P})$ as the maximum and minimum real part of its eigenvalues, respectively. Define L as the Laplace transformation operator and L^{-1} as its inverse operator.

Lemma 1: For system $Y(s) = U(s)/(s+\lambda)^n$ ($\lambda > \lambda_{\max}(\boldsymbol{P}), n \in \mathbb{N}_+$) where $Y(s) \triangleq L[y(t)]$ and $U(s) \triangleq L[u(t)]$. If there exists $\theta \geq 0$ such that $|u(t)| \leq \theta$, then $\lim_{t\to\infty}|y^{(i)}(t)| \leq \frac{\lambda_{\max}(\boldsymbol{P})}{\sqrt{\lambda_{\min}(\boldsymbol{P})}}\theta\frac{\lambda^{-n+1+i}}{\sqrt{\lambda-\lambda_{\max}(\boldsymbol{P})}}$ $(i = 0, 1, \ldots, n-1)$.

Proof: The relationship between y and u in time domain is $y^{(n)} + n\lambda y^{(n-1)} + \cdots + C_n^i\lambda^i y^{(n-i)} + \cdots + \lambda^n y = u$. Letting $x_i \triangleq \lambda^{-i+1}y^{(i-1)}$ $(i = 1, 2, \ldots, n)$, the original system is then rewritten in a compact form as follows:

$$\dot{\boldsymbol{x}} = \lambda\boldsymbol{A}\boldsymbol{x} + \lambda^{-n+1}\boldsymbol{B}u \tag{12}$$

where $\boldsymbol{x} \triangleq [\, x_1 \; x_2 \; \cdots \; x_n \,]^\top$, $\boldsymbol{A}$ is defined before and $\boldsymbol{B} \triangleq [\, \boldsymbol{0}_{1\times(n-1)} \;\; 1_{1\times 1} \,]^\top$.

Construct a candidate Lyapunov function $V(\boldsymbol{x}) \triangleq \boldsymbol{x}^\top\boldsymbol{P}\boldsymbol{x}$. Taking derivative of $V(x)$ along system (12), we have

$$\begin{aligned}
\dot{V}(\boldsymbol{x}) &= -\lambda\|\boldsymbol{x}\|^2 + 2\boldsymbol{x}^\top\boldsymbol{P}\boldsymbol{B}\lambda^{-n+1}u \\
&\leq -\lambda\|\boldsymbol{x}\|^2 + \lambda_{\max}(\boldsymbol{P})(\|\boldsymbol{x}\|^2 + \lambda^{2(-n+1)}\theta^2) \\
&\leq [-\lambda + \lambda_{\max}(\boldsymbol{P})]\|\boldsymbol{x}\|^2 + \lambda_{\max}(\boldsymbol{P})\lambda^{2(-n+1)}\theta^2 \\
&\leq -aV(\boldsymbol{x}) + b
\end{aligned}$$

where $a \triangleq \lambda/\lambda_{\max}(\boldsymbol{P}) - 1 > 0$ and $b \triangleq \lambda_{\max}(\boldsymbol{P})\lambda^{2(-n+1)}\theta^2$.

According to the comparison lemma, we have $V(\boldsymbol{x}) \leq b/a + \exp(-at)[V(0) - b/a]$. Since $V(\boldsymbol{x}) \geq \lambda_{\min}(\boldsymbol{P})\|\boldsymbol{x}\|^2$, we then have $\|\boldsymbol{x}\|^2 \leq \{b/a + \exp(-at)[V(0) - b/a]\}/\lambda_{\min}(\boldsymbol{P})$. As such, $\lim_{t\to\infty}\|\boldsymbol{x}\| \leq \left[\frac{b}{a\lambda_{\min}(\boldsymbol{P})}\right]^{0.5} = \frac{\lambda_{\max}(\boldsymbol{P})}{\sqrt{\lambda_{\min}(\boldsymbol{P})}}\theta\frac{\lambda^{-n+1}}{\sqrt{\lambda-\lambda_{\max}(\boldsymbol{P})}}$.

With the definition of $\boldsymbol{x}$ in mind, we have $\lim_{t\to\infty}|y^{(i)}| = \lambda^i\lim_{t\to\infty}|x_{i+1}| \leq \lambda^i\lim_{t\to\infty}\|\boldsymbol{x}\| \leq \frac{\lambda_{\max}(\boldsymbol{P})}{\sqrt{\lambda_{\min}(\boldsymbol{P})}}\theta\frac{\lambda^{-n+1+i}}{\sqrt{\lambda-\lambda_{\max}(\boldsymbol{P})}}$ $(i = 0, 1, \ldots, n-1)$. ■

The proof of the arbitrarily small speed tracking and disturbance estimation errors is presented as follows.

Proof: Without loss of generality, the eigenvalues of $\boldsymbol{\Phi}_{\boldsymbol{e}}$ and $\boldsymbol{\Phi}_{\boldsymbol{x}}$ are chosen as $-\lambda_o$ ($\lambda_o > 0$, N+5 multiples) and $-\lambda_c$ ($\lambda_c > 0$, 2 multiples).

1) First Step (Estimation Error Dynamics):

The estimation error subsystem can be written as follows:

$$\dot{\boldsymbol{e}} = \boldsymbol{\Phi}_{\boldsymbol{e}}\boldsymbol{e} + \boldsymbol{\xi}d$$

where $\boldsymbol{\xi} \triangleq [\, \boldsymbol{0}_{1\times(N+4)} \;\; 1_{1\times 1} \,]^\top$. According to Corollary 1, there exists a constant $\theta \geq 0$ such that $|d^{(i)}| \leq \theta$ $(i = 0, 1, \ldots, N+5)$.

Define $G_{de_3}(s) \triangleq E_3(s)/D(s)$ where $E_3(s) = L[e_3(t)]$ and $D(s) = L[d(t)]$. It is obvious that $G_{de_3}(s) = \boldsymbol{\tau}\boldsymbol{H}^{-1}\boldsymbol{\xi}$ where $\boldsymbol{\tau} \triangleq [\, 1_{1\times 1} \;\; \boldsymbol{0}_{1\times(N+4)} \,]$ and $\boldsymbol{H} \triangleq \boldsymbol{I} - \boldsymbol{\Phi}_{\boldsymbol{e}} = (h_{ij})$. Since $\det(\boldsymbol{H}) = \sum_{i=1}^{N+5}h_{1i}H_{1i} = (s - l_2 + B_v/J + R_s/L_q)H_{11} - H_{12} - H_{14} - H_{15}$ where H_{ij} is the algebraic cofactor of h_{ij}, one gets that $\det(\boldsymbol{H})$ is a $(N+5)$th order monic polynomial and the coefficient of s^{N+4} is $-l_2 + B_v/J + R_s/L_q$. Since the eigenvalues of $\boldsymbol{\Phi}_{\boldsymbol{e}}$ are chosen as $-\lambda_o$, we have $\det(\boldsymbol{H}) = (s+\lambda_o)^{N+5}$ and $l_2 = -\lambda_o(N+5) + B_v/J + R_s/L_q$. Noting that $\boldsymbol{H}^{-1} = \boldsymbol{H}^*/\det(\boldsymbol{H})$ where $\boldsymbol{H}^*$ is the adjoint matrix of $\boldsymbol{H}$ and $\boldsymbol{H}^* = (h_{ij}^*)$, $h_{ij}^* = H_{ji}$, we have $G_{de_3}(s) = h_{1(N+5)}^*/(s+\lambda_o)^{N+5} = H_{(N+5)1}/(s+\lambda_o)^{N+5}$. Since $H_{(N+5)1}$ is independent of l_i $(i = 2, 3, \ldots, N+6)$ and $L^{-1}[H_{(N+5)1}D(s)]$ is also bounded from Corollary 1, then according to Lemma 1, $\lim_{t\to\infty}|e_3^{(i)}| \leq k\theta\frac{\lambda_o^{-N-4+i}}{\sqrt{\lambda_o-\lambda_{\max}(\boldsymbol{P})}}$ $(\lambda_o >$

[1]Please refer to [46] for more detailed information on ISS. Definition 4.7 in Page 175 and Lemma 4.6 and Exercise 4.58 in Page 176 are crucial in the development of the results in Appendix V-A.

$\lambda_{\max}(\boldsymbol{P}), i = 0, 1, \ldots, N+4)$ where k is an independent positive constant.

Define $e_d(t) \triangleq e_4(t) + e_6(t) + e_8(t)$. Noting that $\dot{e}_3 = (l_2 - B_v/J - R_s/L_q)e_3 + e_d = -\lambda_o(N+5)e_3 + e_d$, then $\lim_{t\to\infty}|e_d| \leq \lim_{t\to\infty}|e_3{}^{(1)}| + (N+5)\lambda_o \lim_{t\to\infty}|e_3| \leq \tilde{k}\theta \frac{\lambda_o{}^{-N-3}}{\sqrt{\lambda_o - \lambda_{\max}(\boldsymbol{P})}}$ where $\tilde{k}$ is also an independent positive constant. Therefore, the ultimate bound for e_3 and e_d can be made arbitrarily small by magnifying λ_o.

2) Second Step (Tracking Error Dynamics):

The state subsystem is written as follows:

$$\dot{\boldsymbol{x}} = \boldsymbol{\Phi}_{\boldsymbol{x}}\boldsymbol{x} + \tilde{\boldsymbol{\xi}}\tilde{d}$$

where $\tilde{\boldsymbol{\xi}} \triangleq [0\ 1]^\top$ and $\tilde{d} \triangleq k_2/L_q e_3 + e_d$. Obviously, this subsystem is also ISS with regard to $\tilde{d}$. Also, noting that the ultimate bound for $\tilde{d}$ can be made arbitrarily small by magnifying λ_o, similar with the previous proof, the ultimate bound for the speed tracking error can be made arbitrarily small. ■

REFERENCES

[1] P. Krause, O. Wasynczuk, S. Sudhoff, and S. Pekarek, *Analysis of Electric Machinery and Drive Systems*. Hoboken, NJ, USA: Wiley, 2013.

[2] S. Li and Z. Liu, "Adaptive speed control for permanent-magnet synchronous motor system with variations of load inertia," *IEEE Trans. Ind. Electron.*, vol. 56, no. 8, pp. 3050–3059, Aug. 2009.

[3] S. Chai, L. Wang, and E. Rogers, "A cascade MPC control structure for PMSM with speed ripple minimization," *IEEE Trans. Ind. Electron.*, vol. 60, no. 8, pp. 2978–2987, Aug. 2013.

[4] R. Errouissi, M. Ouhrouche, W.-H. Chen, and A. M. Trzynadlowski, "Robust nonlinear predictive controller for permanent-magnet synchronous motors with an optimized cost function," *IEEE Trans. Ind. Electron.*, vol. 59, no. 7, pp. 2849–2858, Jul. 2012.

[5] W.-C. Gan and L. Qiu, "Torque and velocity ripple elimination of AC permanent magnet motor control systems using the internal model principle," *IEEE/ASME Trans. Mechatronics*, vol. 9, no. 2, pp. 436–447, Jun. 2004.

[6] H. Sira-Ramírez, J. Linares-Flores, C. García-Rodríguez, and M. A. Contreras-Ordaz, "On the control of the permanent magnet synchronous motor: An active disturbance rejection control approach," *IEEE Trans. Control Syst. Technol.*, vol. 22, no. 5, pp. 2056–2063, Sep. 2014.

[7] J. Shi and S. Li, "Analysis and compensation control of dead-time effect on space vector PWM," *J. Power Electron.*, vol. 15, no. 2, pp. 431–442, Mar. 2015.

[8] W. Qian, S. K. Panda, and J.-X. Xu, "Torque ripple minimization in PM synchronous motors using iterative learning control," *IEEE Trans. Power Electron.*, vol. 19, no. 2, pp. 272–279, Mar. 2004.

[9] M. Ruderman, A. Ruderman, and T. Bertram, "Observer-based compensation of additive periodic torque disturbances in permanent magnet motors," *IEEE Trans. Ind. Informat.*, vol. 9, no. 2, pp. 1130–1138, May 2013.

[10] H. Liu and S. Li, "Speed control for PMSM servo system using predictive functional control and extended state observer," *IEEE Trans. Ind. Electron.*, vol. 59, no. 2, pp. 1171–1183, Feb. 2012.

[11] Y.-R. Mohamed, "Design and implementation of a robust current-control scheme for a PMSM vector drive with a simple adaptive disturbance observer," *IEEE Trans. Ind. Electron.*, vol. 54, no. 4, pp. 1981–1988, Aug. 2007.

[12] K.-H. Kim and M.-J. Youn, "A nonlinear speed control for a PM synchronous motor using a simple disturbance estimation technique," *IEEE Trans. Ind. Electron.*, vol. 49, no. 3, pp. 524–535, Jun. 2002.

[13] I.-C. Baik, K.-H. Kim, and M.-J. Youn, "Robust nonlinear speed control of PM synchronous motor using boundary layer integral sliding mode control technique," *IEEE Trans. Control Syst. Technol.*, vol. 8, no. 1, pp. 47–54, Jan. 2000.

[14] T. D. Do, H. H. Choi, and J.-W. Jung, "$\theta-$D approximation technique for nonlinear optimal speed control design of surface-mounted PMSM drives," *IEEE/ASME Trans. Mechatronics*, vol. 20, no. 4, pp. 1822–1831, Aug. 2015.

[15] J. Yang, S. Li, J. Su, and X. Yu, "Continuous nonsingular terminal sliding mode control for systems with mismatched disturbances," *Automatica*, vol. 49, no. 7, pp. 2287–2291, Jul. 2013.

[16] H. Chaoui and P. Sicard, "Adaptive fuzzy logic control of permanent magnet synchronous machines with nonlinear friction," *IEEE Trans. Ind. Electron.*, vol. 59, no. 2, pp. 1123–1133, Feb. 2012.

[17] A. Isidori and C. Byrnes, "Output regulation of nonlinear systems," *IEEE Trans. Automat. Control*, vol. 35, no. 2, pp. 131–140, Feb. 1990.

[18] C. I. Byrnes, F. D. Priscoli, and A. Isidori, *Output Regulation of Uncertain Nonlinear Systems*, Boston, MA, USA: Birkhauser, 1997.

[19] W.-H. Chen, "Harmonic disturbance observer for nonlinear systems," *J. Dyn. Syst. Meas. Control*, vol. 125, no. 1, pp. 114–117, Mar. 2003.

[20] J. Yang, W.-H. Chen, S. Li, L. Guo, and Y. Yan, "Disturbance/uncertainty estimation and attenuation techniques in PMSM drives–A survey," *IEEE Trans. Ind. Electron.*, vol. 64, no. 4, pp. 3273–3285, Apr. 2017.

[21] T. M. Jahns and W. L. Soong, "Pulsating torque minimization techniques for permanent magnet AC motor drives-A review," *IEEE Trans. Ind. Electron.*, vol. 43, no. 2, pp. 321–330, Apr. 1996.

[22] N. Bianchi and S. Bolognani, "Design techniques for reducing the cogging torque in surface-mounted PM motors," *IEEE Trans. Ind. Appl.*, vol. 38, no. 5, pp. 1259–1265, Sep. 2002.

[23] T. Sebastian, "Temperature effects on torque production and efficiency of PM motors using Ndfeb magnets," *IEEE Trans. Ind. Appl.*, vol. 31, no. 2, pp. 353–357, Mar. 1995.

[24] A. Ferrah, P. J. Hogben-Laing, K. J. Bradley, G. M. Asher, and M. S. Woolfson, "The effect of rotor design on sensorless speed estimation using rotor slot harmonics identified by adaptive digital filtering using the maximum likelihood approach," in *Proc. IEEE Ind. Appl. Soc. Annu. Meeting Conf.*, New Orleans, LA, USA, Oct. 1997, pp. 128–135.

[25] S.-H. Hwang and J.-M. Kim, "Dead time compensation method for voltage-fed PWM inverter," *IEEE Trans. Energy Convers.*, vol. 25, no. 1, pp. 1–10, Mar. 2010.

[26] R. Xiong, H. He, F. Sun, and K. Zhao, "Evaluation on state of charge estimation of batteries with adaptive extended Kalman filter by experiment approach," *IEEE Trans. Veh. Technol.*, vol. 62, no. 1, pp. 108–117, Jan. 2013.

[27] D.-W. Chung and S.-K. Sul, "Analysis and compensation of current measurement error in vector-controlled AC motor drives," *IEEE Trans. Ind. Appl.*, vol. 34, no. 2, pp. 340–345, Mar. 1998.

[28] W. Carter, "Mechanical factors affecting electrical drive performance," *IEEE Trans. Ind. Gen. Appl.*, vol. IGA-5, no. 3, pp. 282–290, May 1969.

[29] K. Meessen, P. Thelin, J. Soulard, and E. Lomonova, "Inductance calculations of permanent-magnet synchronous machines including flux change and self- and cross-saturations," *IEEE Trans. Magn.*, vol. 44, no. 10, pp. 2324–2331, Oct. 2008.

[30] C. Zhang, Y. Yan, A. Narayan, and H. Yu, "Practically oriented finite-time control design and implementation: Application to series elastic actuator," *IEEE Trans. Ind. Electron.*, vol. 65, no. 5, pp. 4166–4176, May 2018.

[31] K. Ohnishi, M. Shibata, and T. Murakami, "Motion control for advanced mechatronics," *IEEE/ASME Trans. Mechatronics*, vol. 1, no. 1, pp. 56–67, Mar. 1996.

[32] H. Olsson, K. Åström, C. Canudas de Wit, M. Gäfvert, and P. Lischinsky, "Friction models and friction compensation," *Eur. J. Control*, vol. 4, no. 3, pp. 176–195, Dec. 1998.

[33] T. Murakami, F. Yu, and K. Ohnishi, "Torque sensorless control in multidegree-of-freedom manipulator," *IEEE Trans. Ind. Electron.*, vol. 40, no. 2, pp. 259–265, Apr. 1993.

[34] H. Olsson, "Control systems with friction," Ph.D. dissertation, Dept. Automat. Control, Lund Univ., Lund, Sweden, 1996.

[35] Z. Ding, "Asymptotic rejection of unmatched general periodic disturbances in a class of nonlinear systems," *IET Control Theory Appl.*, vol. 2, no. 4, pp. 269–276, Apr. 2008.

[36] K. Ohishi, K. Ohnishi, and K. Miyachi, "Torque-speed regulation of DC motor based on load torque estimation method," in *Proc. JIEE/Int. Power Electron. Conf.*, 1983, pp. 1209–1218.

[37] K. Ohishi, M. Nakao, K. Ohnishi, and K. Miyachi, "Microprocessor-controlled DC motor for load-insensitive position servo system," *IEEE Trans. Ind. Electron.*, vol. IE-34, no. 1, pp. 44–49, Feb. 1987.

[38] T. Umeno and Y. Hori, "Robust speed control of DC servomotors using modern two degrees-of-freedom controller design," *IEEE Trans. Ind. Electron.*, vol. 38, no. 5, pp. 363–368, Oct. 1991.

[39] E. Sariyildiz and K. Ohnishi, "An adaptive reaction force observer design," *IEEE/ASME Trans. Mechatronics*, vol. 20, no. 2, pp. 750–760, Apr. 2015.

[40] E. Sariyildiz, G. Chen, and H. Yu, "A unified robust motion controller design for series elastic actuators," *IEEE/ASME Trans. Mechatronics*, vol. 22, no. 5, pp. 2229–2240, Oct. 2017.

[41] W.-H. Chen, "Disturbance observer based control for nonlinear systems," *IEEE/ASME Trans. Mechatronics*, vol. 9, no. 4, pp. 706–710, Dec. 2004.
[42] W.-H. Chen, J. Yang, L. Guo, and S. Li, "Disturbance-observer-based control and related methods–An overview," *IEEE Trans. Ind. Electron.*, vol. 63, no. 2, pp. 1083–1095, Feb. 2016.
[43] Z. Gao, "Scaling and bandwidth-parameterization based controller tuning," in *Proc. Amer. Control Conf.*, Denver, CO, USA, Jun. 2003, pp. 4989–4996.
[44] T. Tarczewski and L. M. Grzesiak, "Constrained state feedback speed control of PMSM based on model predictive approach," *IEEE Trans. Ind. Electron.*, vol. 63, no. 6, pp. 3867–3875, Jun. 2016.
[45] B. Francis and W. Wonham, "The internal model principle of control theory," *Automatica*, vol. 12, no. 5, pp. 457–465, Sep. 1976.
[46] H. Khalil, *Nonlinear Systems*, 3rd ed. Upper Saddle River, NJ, USA: Prentice-Hall, 2002.

Yunda Yan (S'15) was born in Yixing, China, in 1990. He received the B.Sc. degree from the School of Automation, Southeast University, Nanjing, China, in 2013, and is currently working toward the Ph.D. degree in control theory and control engineering from the School of Automation, Southeast University, under the guidance of Profs. S. Li and J. Yang.

He was a Visiting Student in the Department of Biomedical Engineering, National University of Singapore, Singapore, under the guidance of Prof. H. Yu from October 2016 to October 2017. He is currently a Visiting Student with the Department of Aeronautical and Automotive Engineering, Loughborough University, Loughborough, U.K., under the guidance of Dr. C. Liu and Prof. W.-H. Chen. His research interests include the development of predictive control methods, dynamic high-gain control methods, and disturbance modeling, and estimation approaches and their applications in motion control systems.

Jun Yang (M'11) received the B.Sc. degree from the Department of Automatic Control, Northeastern University, Shenyang, China, in 2006, and the Ph.D. degree in control theory and control engineering from the School of Automation, Southeast University, Nanjing, China, in 2011.

He is currently an Associate Professor with the School of Automation, Southeast University. His current research interests include disturbance estimation and compensation, advanced control theory, and its application to flight control systems and motion control systems.

Dr. Yang is an Associate Editor for the *Transactions of the Institute of Measurement and Control*. He was the recipient of the ICI Prize for best paper of *Transactions of the Institute of Measurement and Control* in 2016.

Zhenxing Sun (M' 16) received the B.Eng. degree in electrical engineering from Southeast University, Nanjing, in 2007, the M.Eng. degree in control theory and control engineering from Nanjing Tech University, Nanjing, in 2012, and the Ph.D. degree in control theory and control engineering from Southeast University, in 2017.

He is currently with the Advanced Research Center, National University of Singapore, Singapore, as a Visiting Scholar. Since December 2017, he has been a Lecturer with the College of Electrical Engineering and Control Science, Nanjing Tech University. His main research focuses on advanced control theory with applications to servo, robot, and other mechanical systems.

Chuanlin Zhang (M'14) received the B.S. degree in mathematics and the Ph.D. degree from the School of Automation, Southeast University, Nanjing, China, in 2008 and 2014, respectively.

He was a Visiting Ph.D. Student in the Department of Electrical and Computer Engineering, University of Texas at San Antonio, San Antonio, TX, USA, from 2011 to 2012; and a Visiting Scholar at the Energy Research Institute, Nanyang Technological University, Singapore, from 2016 to 2017. He is currently with the Advanced Robotics Center, National University of Singapore, Singapore, as a Visiting Scholar. Since 2014, he has been with the College of Automation Engineering, Shanghai University of Electric Power, Shanghai, China, where he is currently an Associate Professor. He is the principal investigator of several research projects, including Leading Talent Program of Shanghai Science and Technology Commission, Chenguang Program, by the Shanghai Municipal Education Commission, etc. His research interests include nonlinear system control theory and applications for power systems, where he has authored and co-authored more than 25 journal papers.

Dr. Zhang was the recipient of the Best Poster Paper Award from the 3rd International Federation of Automatic Control International Conference on Intelligent Control and Automation Science (2013).

Shihua Li (M'05–SM'10) was born in Pingxiang, China, in 1975. He received the bachelor's, master's, and Ph.D. degrees in automatic control from Southeast University, Nanjing, China, in 1995, 1998, and 2001, respectively.

Since 2001, he has been with the School of Automation, Southeast University, where he is currently a Professor and the Director of Mechatronic Systems Control Laboratory. He has authored or co-authored more than 200 technical papers and two books. His main research interests include modeling, analysis, and nonlinear control theory with applications to mechatronic systems.

Prof. Li is the Vice Chairman of the IEEE Control Systems Society Nanjing Chapter. He serves as an Associate Editor or Editor for the *International Journal of Robustand Nonlinear Control*; *IET Power Electronics; the International Journal of Control, Automation, and Systems*; and the *International Journal of Electronics*, and as a Guest Editor for the IEEE TRANSACTIONS ON INDUSTRIAL ELECTRONICS, the *International Journal of Robust and Nonlinear Control,* and *IET Control Theory and Applications*.

Haoyong Yu (M'10) received the Ph.D. degree in mechanical engineering from the Massachusetts Institute of Technology, Cambridge, MA, USA, in 2002.

He was a Principal Member of Technical Staff at the Defence Science Organisation National Laboratories, Singapore, until 2002. He is currently an Associate Professor with the Department of Biomedical Engineering and a Principal Investigator with the Singapore Institute of Neurotechnology, National University of Singapore, Singapore. His research interests include medical robotics, rehabilitation engineering and assistive technologies, system dynamics, and control.

Dr. Yu was the recipient of the Outstanding Poster Award at the IEEE Life Sciences Grand Challenges Conference 2013. He has served on a number of IEEE conference organizing committees.